DMD Fast Forward. Published on January 18, 2018 as DOI: 10.1124/dmd.117.077511
This article has not been copyedited and formatted. The final version may differ from this version.

DMD # 77511

Title: Metabolism and Disposition of a Novel Selective α7 Neuronal Acetylcholine Receptor Agonist ABT-126 in Humans: Characterization of the Major Roles for Flavin-containing Monooxygenases and UDP-glucuronosyl Transferase 1A4 and 2B10 in Catalysis

Authors: Hong Liu[1], David M. Stresser, Melissa J. Michmerhuizen, Xiaofeng Li, Ahmed A. Othman, Aimee D. Reed, Michael R. Schrimpf, Jens Sydor, Anthony J. Lee

Bioanalysis and Biotransformation (H.L., M.J.M., J.S., A.J.L.); DMPK and Translational Modeling (D.M.S., X.L.); Process Chemistry (A.D.R.); Discovery Chemistry and Technology (M.R.S.); Clinical Pharmacology and Pharmacometrics (A.A.O.), Research & Development, AbbVie, North Chicago, Illinois

DMD Fast Forward. Published on January 18, 2018 as DOI: 10.1124/dmd.117.077511
This article has not been copyedited and formatted. The final version may differ from this version.

Running Title: Metabolism and disposition of ABT-126 in humans.

Corresponding author: Dr. Hong Liu

[1]Present address: Novartis Institutes for BioMedical Research (NIBR) Pharmacokinetic Sciences, Cambridge, MA 02139. Email: hong.liu@novartis.com

Number of text pages: 33

Number of tables: 5

Number of figures: 8

Number of reference: 33

Number of words in the Abstract: 245

Number of words in the Introduction: 432

Number of words in the Discussion: 1181

ABBREVIATIONS: AChEIs, acetylcholine esterase inhibitors; AD, Alzheimer's disease; AUC, area under the curve; cpm, counts per minute; CYP, cytochrome P450; CID, collision-induced dissociation; K_2-EDTA, di-potassium ethylenediaminetetraacetate; dpm, disintegrations per minute; FDA, U.S. Food and Drug Administration; FMO, flavin-containing monooxygenase; HPLC, high-performance liquid chromatography; HLM, human liver microsomes; HKM, human kidney microsomes; LLOQ, lower limit of quantitation; LSC, liquid scintillation counting; μCi, microcuries; NADHP, nicotinamide adenine dinucleotide phosphate; nAChRs, neuronal acetylcholine receptors; ppm, parts per million; PK/PD, pharmacokinetic/pharmacodynamics; QD, daily dose; SPE, solid phase extraction; SD, standard deviation; UGT, uridine 5'-diphospho-glucuronosyltransferase

Abstract

Mass balance, metabolism and excretion of ABT-126, an α7 nAChRs agonist, were characterized in healthy male subjects (n=4) following a single 100 mg (100 μCi) oral dose. The total recovery of the administered radioactivity was 94.0% (±2.09%) with 81.5% (± 10.2%) in urine and 12.4% (± 9.3%) in feces. Metabolite profiling indicated that ABT-126 had been extensively metabolized with 6.6% of the dose remaining as unchanged parent drug in urine. Parent drug accounted for 12.2% of the administered radioactivity in feces. The primary metabolic transformations of ABT-126 involved aza-adamantane *N*-oxidation (M1, 50.3% in urine) and aza-adamantane *N*-glucuronidation (M11, 19.9% in urine). M1 and M11 were also major circulating metabolites, accounting for 32.6% and 36.6% of the drug related material in plasma, respectively. These results demonstrated that ABT-126 is primarily eliminated by hepatic metabolism followed by urinary excretion. Enzymatic studies suggested M1 formation is primarily mediated by human liver FMO3 and to a lesser extent by human kidney FMO1; M11 is mainly generated by human UGT1A4 while UGT2B10 also contributes to ABT-126 glucuronidation. Species dependent formation of M11 was observed in hepatocytes; M11 was formed in human and monkey hepatocytes, but not in rat and dog hepatocytes suggesting monkey is an appropriate model for predicting fate of compounds undergoing significant *N*-glucuronidation. M1 and M11 are not expected to have clinically relevant on- or off-target pharmacological activities. In summary, this study characterized ABT-126 metabolites in circulation and excreta and the primary elimination pathways of ABT-126 in human.

Introduction

Alzheimer's disease (AD) is a chronic neurodegenerative disease and the most common cause of dementia. As of 2016, an estimated 5.4 million Americans have Alzheimer's disease (Alzheimer's, 2016). The few available treatments for Alzheimer's disease [acetylcholine esterase inhibitors (AChEIs) and *N*-methyl-D-aspartate receptor antagonists] provide temporary improvement in cognition, but none of them slows or stops the damage of neurons that cause Alzheimer's symptoms. There is a clear medical need for new therapy to treat this disease. α7 neuronal acetylcholine receptors (nAChRs) are acetylcholine-gated cation channels that are localized on the brain regions critical to the synaptic plasticity underlying learning and memory. Activation of α7 nAChRs can cause the release of neurotransmitters (γ-aminobutyric acid [GABA], acetylcholine [ACh] and glutamate) important for cognition (Lendvai et al., 2013). Several studies suggest that α7 nAChR plays a significant role in the development of AD pathology (Gotti and Clementi, 2004; Roncarati et al., 2009). The α7 nAChR agonist under development by EnVivo (EVP-6124) has shown the potential in the treatment of AD (Deardorff et al., 2015).

ABT-126 is a potent and selective α7 nAChR agonist with high binding affinity (Ki = 12-14 nM) to α7 nAChRs (human, rat or mouse cortex) (Gault et al., 2016). ABT-126 shows significantly less affinity (>140-fold) toward other nAChR subtypes and muscarinic receptor, and therefore is expected to eliminate the dose-limiting toxicity associated with AChEIs. ABT-126 exhibits a preclinical efficacy profile across multiple cognitive domains of relevance to AD. ABT-126 was evaluated in single-dose and multiple dose phase 1 studies, and doses up to 150 mg once daily (QD) or up to 40 mg twice a day were generally well tolerated (AbbVie internal data). The results from a phase 2a trial indicated that treatment with ABT-126 was associated

with a trend for improvement in cognition in subjects with mild to moderated AD (Gault et al., 2015). However, the subsequent phase 2b trial encompassing a broader dose range didn't demonstrate statistically significant improvement vs a placebo control (Florian et al., 2016; Gault et al., 2016). In another phase 2a trial in subjects with schizophrenia, ABT-126 demonstrated a precognitive effect in nonsmoking subjects, particularly in verbal learning, working memory, and attention (Haig et al., 2016b). A follow-up dose-ranging study showed ABT-126 didn't demonstrate a consistent effect on cognition in nonsmoking subjects with schizophrenia; however, a trend toward a therapeutic effect was observed on negative symptoms (Haig et al., 2016a).

The objectives of the current study were to determine the mass balance, routes of excretion, characterize the major metabolites of ABT-126 in healthy human volunteers and identify the major enzymes catalyzing the biotransformation of ABT-126.

Materials and Methods

Drugs and Reagents

The chemical names for ABT-126, M1, M11, and M12 are 2-((1r,3R,4s,5S,7s)-1-azaadamantan-4-yloxy)-5-phenyl-1,3,4-thiadiazole, ((1s,3R,4s, 5S, 7s)-4-((5-Phenyl-[1,3,4]thiadiazol-2-yl)oxy)-1-azaadamantane-1-oxide), (2S,3S,4S,5R,6S)-3,4,5-trihydroxy-6-((1s,3R,4R,5S,7R)-4-((5-phenyl-1,3,4-thiadiazol-2-yl)oxy)-1-azaadamantan-1-ium-1-yl)tetrahydro-2H-pyran-2-carboxylate, (1s,3R,4S,5S,7S)-4-((5-phenyl-1,3,4-thiadiazol-2-yl)oxy)-1-((2R,3R,4S,5S,6R)-3,4,5-trihydroxy-6-(hydroxymethyl)tetrahydro-2H-pyran-2-yl)-1-azaadamantan-1-ium, respectively. ABT-126, M1, M11, M12 reference standards were supplied by Process Chemistry, AbbVie, Inc (North Chicago, IL) and were used as HPLC and mass spectrometric standards. The synthesis of M1, M11, and M12 were provided in the supplemental data. [^{3}H]ABT-126 was

synthesized in one step by hydrogenolysis of the corresponding bromo precursor (2-((1r,3R,4s,5S,7s)-1-azaadamantan-4-yloxy)-5-(3-bromophenyl)-1,3,4-thiadiazole). Radiochemical purity after HPLC purification of [^{3}H]ABT-126 was >99%. [^{14}C]ABT-126 was synthesized in 3 steps starting from [^{14}C] carbonyl labeled benzoic acid. Purification of the compound by crystallization provided >98% radiochemical purity by HPLC. More detailed synthetic procedures were provided in the supplemental data. Chemical structures of [^{3}H]ABT-126 (T denotes ^{3}H) and [^{14}C]ABT-126 (* denotes ^{14}C) are shown in Figure S1.

All HPLC-grade solvents used for liquid chromatography-tandem mass spectrometry (LC-MS/MS) analysis were purchased from Sigma-Aldrich (St. Louis, MO). The scintillation fluids used for radioanalysis were purchased from PerkinElmer (Waltham, MA). Cryopreserved hepatocytes from male Sprague-Dawley (SD) (Lot TIJ), male beagle dog (Lot BWX), male cynomolgus monkey (Lot EHH), and human (Lot AOI) were purchased from Celsis In Vitro Technologies Inc. (Baltimore, MD). Corning® Supersomes™ prepared from control baculovirus-infected insect cells expressing human CYP isoforms 1A2, 2A6, 2B6, 2C8, 2C9, 2C18, 2C19, 2D6, 2E1, 3A4, FMO isoforms FMO1, FMO3, FMO5 and UGT isoforms 1A1, 1A3, 1A4, 1A6, 1A7, 1A9, 1A10, 2B4, 2B7, 2B10, 2B15, and 2B17 were obtained from Corning Life Sciences (Woburn, MA). Pooled human liver and kidney microsomes were obtained from Sekisui Xenotech (Kansas City, KS).

Clinical Study

The clinical study was conducted at Covance Laboratories Inc., in conjunction with the Covance Clinical Research Unit (Madison, WI). This was a phase 1, single radiolabeled dose, open-label, single center, mass balance study. The study was conducted in accordance with Good Clinical Practice guidelines and ethical principles that have their origin in the Declaration of

Helsinki. The study protocol was approved by the institutional review board and all subjects provided written informed consent before any study-related procedures were performed. The radioactive dose of 100 μCi was chosen so that the radiation burden for healthy volunteers remained below the allowable United States FDA whole body exposure limits of 3000 mRem for a single dose of radioactivity. The single dose of 100 mg ABT-126 for this open-label study was selected based on the available pharmacokinetic/pharmacodynamics (PK/PD) and safety information. In a Phase 1 study of ABT-126 in healthy adult subjects, doses up to 150 mg QD for up to 10 days had been safe and well-tolerated with no clinically significant adverse effects reported (AbbVie Internal data).

A total of four male subjects, in general good health, were selected to participate in the study according to predetermined criteria. On the morning of Study Day 1, subjects received a single oral dose of [^{14}C]ABT-126 with approximately 240 mL of water approximately 30 minutes after completion of a standardized breakfast. Subjects were confined to the study site and supervised beginning on Study Day-1 and continuing through 192 hours after dosing and completion of study activities. Subjects were released from the study site at any time after 192 hours post dose, once either of the following conditions was met: 1) greater than 90% of the total radioactivity was recovered, or 2) less than 1% of the radioactive dose was recovered in two consecutive 24-hour collection periods.

Blood samples were collected by venipuncture into vacutainer collection tubes containing di-potassium ethylenediaminetetraacetate (K_2-EDTA) at the following time points: 0 hour (predose), 0.5, 1, 2, 3, 4, 6, 9, 12, 16, 24, 48, 72, 96, 120, 144, 168, 192 and 216 hours after [^{14}C]ABT-126 dosing. Plasma was separated via centrifugation and stored at –70°C.

Urine samples were collected predose and over the following intervals: 0 to 8, 8 to 24, 24 to 48, 48 to 72, 72 to 96, 96 to 120, 120 to 144, 144 to 168, 168 to 192 and 192 to 216 hours after [^{14}C]ABT-126 dosing. Aliquots of the urine were frozen and maintained at –70°C prior to total radioactivity determination and metabolite profile and identification.

Fecal samples were collected predose (upon check-in before dosing) and over the following intervals after dosing: 0 to 24, 24 to 48, 48 to 72, 72 to 96, 96 to 120, 120 to 144, 144 to 168, 168 to 192 and 192 to 216 hours after dosing of [^{14}C]ABT-126 on Study Day 1. All feces collected during a collection interval were kept frozen at -70 °C prior to total radioactivity analysis and metabolite profile and identification.

Total Radioactivity Measurement by Liquid Scintillation Counting (LSC)

All sample combustions were conducted in a Model 307 Sample Oxidizer (Packard Instrument Company) and the resulting $^{14}CO_2$ was trapped in Carbo-Sorb and mixed with aqueous mounting medium (PermaFluor; PerkinElmer). Oxidation efficiency was evaluated on each day of sample combustion by analyzing a commercial radiolabeled standard both directly in scintillation cocktail and by oxidation. Acceptance criteria were combustion recoveries of 95 to 105%. EcoLite(+) scintillation cocktail was used for samples analyzed directly. All samples were analyzed for radioactivity in Model 2900TR liquid scintillation counters (Packard Instrument Company) for at least 5 minutes or 100,000 counts. Each sample was homogenized or mixed before radioanalysis (unless the entire sample was used for analysis). All samples were analyzed in duplicate if sample size allowed. If results from sample replicates (calculated as ^{14}C dpm/g sample) differed by more than 10% from the mean value and sample aliquots had radioactivity greater than 200 dpm, the sample was rehomogenized or remixed and reanalyzed (if the sample size permitted). Scintillation counting data (cpm) were automatically corrected for

counting efficiency using the external standardization technique and an instrument-stored quench curve generated from a series of sealed quenched standards.

Blood samples were mixed and duplicate weighed aliquots (approximately 0.1 to 0.2 g) were combusted and analyzed by LSC. The representative lower limit of quantitation (LLOQ) for blood was 49.6 ng equivalents/g. Plasma samples were mixed and duplicate weighed aliquots (approximately 0.2 g) were analyzed directly by LSC. The representative LLOQ for plasma was 40.1 ng equivalents/g. The urine samples were mixed and duplicate weighed aliquots (approximately 0.2 g) were analyzed directly by LSC. The representative LLOQ for urine was 35.9 ng equivalents/g. Fecal samples were combined by subject at 24-hour intervals and the weight of each combined sample was recorded. A weighed amount of water was added and the sample was mixed. The sample was either immediately homogenized or removed from the freezer and homogenized using a probe-type homogenizer. Duplicate weighed aliquots (approximately 0.2 g) were combusted and analyzed by LSC. The representative LLOQ for feces was 253 ng equivalents/g.

Sample Preparation for Metabolite Profiling

Plasma samples were thawed at room temperature and pooled across subjects at selected time points or AUC pooled per subject utilizing the method of Hamilton et al (Hamilton et al., 1981). Plasma samples were processed using a solvent extraction method. In brief, the pooled plasma sample (4 mL) was extracted with a four-fold volume of acetonitrile/methanol (3/1, v/v), followed by sonication and vortex mixing. The sample was centrifuged at 1875 g for 30 minutes at 4°C. The protein pellets were extracted using 8 mL of acetonitrile/methanol (3/1, v/v), followed by centrifugation at 1875 g. The supernatants were combined and concentrated to about 200 µL under a stream of nitrogen; the residue was diluted with 200 µL of methanol/0.1%

formic acid in water (1/1, v/v) before HPLC-MS-radioflow detection. An aliquot of the reconstituted sample was subjected to LSC counting to determine the total radioactivity recovery. Aliquot of the reconstituted sample was transferred to HPLC autosampler vials for LC-MS analysis. The radioactivity recovery in the processed plasma samples ranged from 80-100%.

An equal volume of fecal homogenate was pooled across subjects at each time point before processing. The pooled fecal samples (30-40 mL) were processed using solvent extraction with 20 mL of acetonitrile/methanol (3/1, v/v), followed by centrifugation at 1875 g for 30 minutes at 4°C. The extraction was repeated with 10 mL of acetonitrile/methanol (3/1, v/v), followed by centrifugation at 1875 g for 30 minutes at 4°C. Aliquots of extracted sample were subjected to LSC counting for total radioactivity. All the supernatants were combined and concentrated under nitrogen flow at room temperature. The concentrated samples (~10 mL) were combined with 5 mL of acetonitrile/methanol (3/1, v/v). The resulting solution was vortexed, sonicated and centrifuged at 1875 g for 30 minutes at 4°C. An aliquot was subjected to HPLC-MS-radioflow detection analysis for metabolite characterization. An aliquot of solution was subjected to LSC radiocounting for extraction recovery calculation. The overall radioactivity recovery for fecal samples ranged from 61-100%.

An equal volume of urine sample was pooled across subjects at each time point and processed by centrifugation at 1875 g for 30 minutes at 4°C. Aliquots of supernatant at 0-8, 8-24, 24-48, 48-72 and 72-96 hours were used directly for HPLC-MS-radioflow detection. Pooled urine samples at 96-120, 120-144, 144-168, 168-192 and 192-216 hours were concentrated under nitrogen flow at room temperature to ~1.7 mL for analysis. The overall radioactivity recovery for urine samples ranged from 84-100%.

Method for Metabolite Profiling and Identification

HPLC separation of ABT-126 and metabolites in human plasma, urine, and feces was achieved using a Thermo Accela UHPLC system (Thermo Fisher Scientific, Waltham, MA) which consisted of an Accela autosampler and 1250 series binary pump. For in vitro samples from hepatocytes and enzyme phenotyping studies, HPLC separation was achieved using an Agilent 1100 Series (Thermo Fisher Scientific, Waltham, MA) which consisted of an autosampler and quaternary pump. Separation for all samples was achieved at room temperature on a Phenomenex Luna C8 (2), 5 µm, 4.6 x 250 mm HPLC column. The HPLC mobile phases consisted of 25 mM ammonium formate (adjusted to pH 3.5 with formic acid) containing 2.5% methanol (solvent A) and 100% acetonitrile (solvent B); the flow rate was maintained at 1.0 mL/minutes. The gradient for human plasma, urine, and feces was as follows: 0-30 minutes, 10-18% solvent B; 30-60 minutes, 18-22% solvent B; 60-61 minutes, 22-90% B; 61-65 minutes, 90% solvent B; 65-66 minutes, 90-10% solvent B; 66-76 minutes, 10% solvent B. The gradient for in vitro samples was as follows: 0-35 minutes, 5-30% solvent B; 35-36 minutes, 30-80% solvent B; 36-40 minutes, 80% B; 40-41 minutes, 80-5% solvent B; 41-51 minutes, 5% solvent B. For samples from human plasma, urine, and feces, the HPLC system was interfaced with a Thermo Fisher LTQ Orbitrap mass spectrometer (Thermo Fisher Scientific, Waltham, MA). The mass spectrometer used for in vitro samples analysis from hepatocytes and enzyme phenotyping studies was a LCQ Deca XP MAX (Thermo Fisher Scientific, Waltham, MA). The MS analyses were conducted using electrospray ionization operated in positive ionization mode. The MS settings were as follows: electrospray ionization voltage, 4.5 kV; capillary temperature, 350°C; capillary voltage, 14 V; tube lens, 105 V. The sheath gas was set to 45.0 arbitrary units, and auxiliary gas to 0 arbitrary unit. The unchanged parent drug and its metabolites were detected using data-dependent, multiple-stage mass analysis, and normalized collision energy of 35% for

both tandem MS (MS^2) and multiple stage MS (MS^3). For sample analysis from human plasma, urine, and feces, the mass resolution was set at 30,000 for full scan and 15,000 for MS^n scan. The instrument was calibrated daily using external calibration reference compounds. Typical mass errors of analytes relative to theoretical masses were less than ± 5 parts per million (ppm) in daily operations. Data acquisition and processing were carried out using Thermo Xcalibur 2.10. Radiolabeled components in plasma, urine, or fecal samples were detected by Perkin Elmer TopCount 96-well LUMA plates (Perkin Elmer, Waltham, MA). The HPLC eluent was split in a ratio of 1 to 4; about 200 µL/minute of flow was diverted to mass spectrometer and ~800 µL/minute flow was collected using Agilent 1100 fraction collection system set at 0.27 minutes interval per well collection. Radiolabeled components from in vitro samples were detected by a Packard 500 TR flow scintillation detector equipped with a 250 µL cell. Data was processed using the Radiomatic™ Flo-one® software v3.65. The scintillant (Perkin Elmer FLO-SINT™ III) flow was maintained at 3 mL/minute.

LC-MS/MS Analysis for *in vitro* Samples

Samples from M1 and M11 formation kinetics were analyzed by multiple reaction monitoring on an LC-MS/MS system consisting of Agilent 1290 HPLC pump (Agilent, Santa Clara, CA), CTC PAL autosampler (Leap Technologies, Carrboro, NC) and an API 5500 MS system equipped with an electrospray ion source and operated by the Analyst software package (Applied Biosystems, Foster City, CA). The source temperature was set to 600 °C. Chromatography was conducted on a Fortis Pace C18 (30 x 2.1 mm) analytical column. The HPLC mobile phases consisted of 0.1% formic acid in water (solvent A) and 0.1% formic acid in acetonitrile (solvent B); the flow rate was maintained at 0.8 mL/minute. The gradient was as follows: 0-0.05 minutes, 5% solvent B; 0.05-0.3 minutes, 5-98% solvent B; 0.3-0.7 minutes,

98% B; 0.7-0.8 minutes, 98-5% solvent B; 0.8-0.9 minutes, 5% solvent B. M1 (*m/z* 329.8→135.9), M11 (*m/z* 490.2→314.1) and internal standard carbutamide (*m/z* 272.2→108.1) were detected in positive ion mode.

Pharmacokinetic Calculations

Values for the pharmacokinetic parameters of total radioactivity, ABT-126, M1, and M11 were determined using noncompartmental methods. Parameters that were estimated included the maximum plasma concentration (C_{max}), the time to C_{max} (T_{max}), and the area under the concentration-time curve from time 0 to the last measureable time point (AUC_t) and to infinite time (AUC_∞).

***In Vitro* Hepatocytes Incubations**

Incubations were performed in duplicate at 37 ^oC in 5% CO_2/95% air, with gentle shaking. Each incubation contained 1 μM [^{3}H]ABT-126 and thawed cryopreserved hepatocytes (500,000 viable cells/mL, 0.5 mL). The reaction was quenched by the addition of 1 mL of acetonitrile/methanol (1/1, v/v) at 0, 0.5, 1, 2, and 4 hour after the addition of [^{3}H]ABT-126. Samples were centrifuged for 30 min at 1279 g (Eppendorf 5810 R centrifuge), and resulting supernatants were analyzed by HPLC-MS/MS with radioflow detection. Detailed analytical conditions are described in the "Methods for Metabolite Profiling and Identification" section.

CYP/FMO Phenotyping and Kinetics

The in vitro oxidative metabolism of [^{3}H]ABT-126 was investigated with a panel of recombinant human CYP enzymes (CYP1A2, 2A6, 2B6, 2C8, 2C9, 2C18, 2C19, 2D6, 2E1, 3A4) and FMO enzymes (FMO1, FMO3, and FMO5). An incubation mixture (200 μL) contained individual P450 isoforms at 100 pmol/mL (200 pmol/mL for CYP2C8) or FMO1, FMO3, FMO5 at 0.5 mg protein/mL, respectively and [^{3}H]ABT-126 (1 μM) in 50 mM potassium phosphate

buffer at pH 7.4. The reaction was initiated by addition of 1 mM of NADPH and incubated at 37 ^{o}C for 60 minutes. The reaction was terminated by addition of 200 µL of acetonitrile/methanol (1/1, v/v). After vortexing and centrifugation, the supernatants were analyzed by HPLC analysis with radioactivity detection. Detailed analytical conditions are described in the "Method for Metabolite Profiling and Identification" section.

To determine enzyme kinetic parameters for the formation of M1, incubations containing ABT-126 at varying concentrations (0.3 to 150 µM) were conducted in triplicate with recombinant FMO1 (0.05 mg/mL, 10 minutes) and FMO3 (0.1 mg/mL, 10 minutes) at 37 ^{o}C in 50 mM phosphate buffer in a volume of 200 µL. The incubation conditions were optimized to ensure M1 formation was linear with incubation time and protein concentration. The incubations were initiated with addition of NADPH cofactor (final concentration of 1mM). At the end of the incubation, the reaction mixtures were quenched with 2-fold volume of acetonitrile containing 50 nM of carbutamide (internal standard) and centrifuged at 1811 g for 10 minutes. The supernatants and standards were analyzed by LC-MS/MS. Detailed analytical conditions are described in the "LC-MS/MS Analysis for in vitro Samples" section.

Incubation in HLM and HKM and Thermal Inactivation Studies

To further investigate FMO contributions to the oxidative metabolism of ABT-126, incubations were conducted with HLM or HKM. An incubation mixture (360 µL) contained 0.5 mg/mL HLM or HKM (untreated and thermally treated) and ABT-126 (150 µM) in 50 mM potassium phosphate buffer at pH 7.4, and were conducted in triplicate. The reaction was initiated by addition of 10 mM of NADPH (40 µL, final concentration of 1 mM) and incubated at 37 ^{o}C. After 0, 15, 30 and 60 minutes, the reaction was terminated by transferring a 25 µL aliquot of the incubation mixture into 125 µL of acetonitrile, containing 50 nM carbutamide as

internal standard. After vortexing and centrifugation, the supernatants were analyzed by HPLC. A standard curve of M1 was prepared under same conditions. Detailed analytical conditions are described in the "Method for Metabolite Profiling and Identification" section. Thermal inactivation of microsomal FMO: The FMO enzyme(s) in HLM or HKM reagents was thermally inactivated according to the method of Grothusen et al (1996). Suspensions of HLM and HKM (diluted to 0.56 mg/mL in 50 mM phosphate buffer) were placed in a 50 °C water bath. After 90 seconds, the tubes were immediately chilled in ice-cold water.

UGT Phenotyping and Kinetics

The in vitro glucuronidation of ABT-126 was investigated with a panel of recombinant human UGT enzymes (UGT1A1, 1A3, 1A4, 1A6, 1A7, 1A9, 1A10, 2B4, 2B7, 2B10, 2B15, and 2B17). An incubation mixture contained individual UGT at 1 mg/mL, ABT-126 (0.5-1 μM), MgCl2 [1 mM or 10 mM (UGT2B10 only)], and 50 μg/mL or 5 μg/mL (UGT2B10 only) of alamethicin in 50 mM Tris buffer at pH 7.4. The mixtures were kept at 0 °C for 15 minutes to allow alamethicin to form membrane pores. The reaction was initiated by addition of 5 mM UDPGA and incubated at 37 °C for 60 minutes. The reaction was terminated by addition of 2X volume of acetonitrile/methanol (1/1, v/v). After centrifugation, supernatants were analyzed by high-performance liquid chromatography (HPLC) analysis with radiometric detection or LC-MS/MS detection (UGT2B10 only) as described earlier.

To determine enzyme kinetic parameters for the formation of M11, incubations containing ABT-126 at varying concentrations (0.2 μM to 150 μM for UGT1A4 and 0.5 to 50 μM for UGT2B10) were conducted in triplicate with recombinant UGT1A4 (0.1 mg/mL, 20 minutes) and UGT2B10 (0.15 mg/mL, 20 minutes) at 37 ^{o}C in 50 mM Tris buffer containing 5 mM of UDPGA, 10 mM $MgCl_2$, and 5 μg/mL of alamethicin. The total reaction volume was 80 μL. The

DMD Fast Forward. Published on January 18, 2018 as DOI: 10.1124/dmd.117.077511
This article has not been copyedited and formatted. The final version may differ from this version.

incubation conditions were optimized to ensure formation of M11 was linear with incubation time and protein concentration. At the end of the incubations, the reaction mixtures were quenched with 160 µL acetonitrile containing 50 nM of carbutamide (internal standard) and centrifuged at 1811 g for 15 minutes. The supernatants were analyzed by LC-MS/MS. Detailed analytical conditions are described in the "LC-MS/MS Analysis for in vitro Samples" section.

Enzyme kinetic analysis

Enzyme kinetic analysis was performed using GraphPad Prism software. Data were fit to a one or two binding site model based on visual inspection of Eadie-Hofstee plots indicating mono- or biphasic kinetics, respectively. Goodness of fit was determined by Akaike information criterion and/or ensuring an even distribution of data points around the fitted line. Individual kinetic parameters were determined using equation 1 (UGT2B10) or equation 2 (UGT1A4):

$$v = \frac{V_{max}[S]}{K_m + [S]} \quad \text{(eq 1)}$$

$$v = \frac{V_{max1}[S]}{K_{m1} + [S]} + \frac{V_{max2}[S]}{K_{m2} + [S]} \quad \text{(eq 2)}$$

Kinetic parameters were used to obtain overall intrinsic clearance (CL_{int}; µL/minute/mg).

Results

Pharmacokinetics

The PK parameters for ABT-126 and its metabolites and for total radioactivity are summarized in Table 1; the PK profiles are shown in Figure 1. The concentration of total radioactivity was measured by LSC, expressed in nanogram-equivalent per gram. The concentrations of ABT-126 were determined using a validated LC-MS/MS bioanalytical method (expressed in units of nanogram per milliliter) and a radioprofiling method (expressed in units of

nanogram-equivalent per gram). The concentration of M1 and M11 were determined using radioprofiling and expressed in units of nanogram-equivalent per gram. The concentrations of ABT-126 determined using a validated LC-MS/MS method were similar with those determined using radioprofiling. ABT-126 reached maximum plasma concentrations (T_{max}) at a median of 4 hours and had a mean C_{max} and $t_{1/2}$ (terminal phase elimination half-life) of 89.7 ng/mL and 33.9 hours, respectively. The maximal plasma concentrations of total radioactivity, M1, and M11 were achieved at 4, 3, and 16 hours post dose, respectively. The estimation of terminal half-lives for total radioactivity, ABT-126 (radioprofiling), M1 and M11 was not conducted due to the absence of measurable radioactivity after 48 hours. M1 and M11 represented about 115% and 128% of parent drug exposure (AUC_{∞}) and accounted for approximately 32.6% and 36.6% of plasma radioactivity (based on AUC_{∞}), respectively.

Excretion of Radioactivity

The mean cumulative percentage of the radioactive dose recovered in urine and feces is illustrated in Figure 2. ABT-126 and related material were primarily excreted in urine with a mean (± SD) recovery of 81.5% (± 10.2%) of the administered dose. Mean (± SD) fecal excretion accounted for 12.4% (± 9.3%) of the administered dose. Total recovery of radioactivity in urine and feces was 94.0% (± 2.09%), with recovery in individual subjects ranging from 91.0-95.9%. The majority of the administered radioactivity was recovered in the first 120 hours post dose (89.3%).

Metabolite Profiles of [^{14}C]ABT-126 in Circulation and Excreta

Plasma

A representative HPLC radiochromatogram of [^{14}C]ABT-126 and its metabolites in pooled human plasma is shown in Figure 3. ABT-126, M1 (*N*-oxide) and M11 (*N*-glucuronide) are

predominant components in human plasma, and metabolite M12 (*N*-glucose conjugate) is present as a minor metabolite. In addition, trace levels of metabolites M3 (di-oxidation), M7 (di-oxidation plus sulfation), M8 (mono-oxidation plus glucuronidation), M10 (mono-oxidation plus cysteine conjugation), and M16 (*N*-oxidation plus glucuronidation) were detected only by LC-MS analysis.

Urine

The representative HPLC radiochromatogram of pooled human urine is shown in Figure 4. The amount of ABT-126 and metabolites in urine, expressed as the mean percentage of the administered dose, is tabulated in Table 2. The administered [^{14}C]ABT-126 was primarily recovered in urine as metabolites (74.6% of the administered dose), whereas 6.6% of the administered dose was recovered as the unchanged parent drug. Similar with the metabolite profile in plasma, the most significant metabolites in urine were M1 and M11, representing 50.3% and 19.9% of the administered dose, respectively. Several minor metabolites were also identified in urine including M3, M10, M12 and M16, each representing <2% of the administered dose. Trace amount of metabolites including M7 and M8 were only detected by LC/MS.

Feces

The representative HPLC radiochromatogram of pooled human feces is shown in Figure 5. The amount of ABT-126 and metabolites in feces, expressed as the mean percentage of the administered dose, is tabulated in Table 2. The administered [^{14}C]ABT-126 was recovered in feces primarily as intact parent drug (12.2% of the administered dose), with 0.2% of the administered dose was recovered M11. Minor metabolites including M1, M3, and M12 were only detected by LC-MS analysis.

Structural Characterization of ABT-126 and Main Metabolites

DMD Fast Forward. Published on January 18, 2018 as DOI: 10.1124/dmd.117.077511
This article has not been copyedited and formatted. The final version may differ from this version.

Metabolites of ABT-126 were characterized using a combination of positive ionization high resolution full scan MS and product ion scan (MS/MS) analyses (Figure S2). The chemical structures of metabolites M1, M11, and M12 were confirmed by comparing its chromatographic retention time and mass spectral fragmentations with those of the reference standards. Chemical structures of other minor metabolites (each <2% of the dose) including M3, M7, M8, M10, and M16 were proposed based on high resolution MS/MS fragmentation pattern analysis. The high resolution product ion mass spectra and proposed structures for these minor metabolites are presented in Supplemental data (Figure S2). The measured accurate masses and characteristic fragment ions are listed in Table 3.

ABT-126. ABT-126 yielded a protonated molecular ion at *m/z* 314.1325 (calculated mass *m/z* 314.1322; $C_{17}H_{20}N_3OS^+$). Collision-induced dissociation (CID) of ABT-126 (*m/z* 314) produced the fragment ions at *m/z* 136.1122 (loss of phenylthiadiazole moiety; $C_9H_{14}N^+$), *m/z* 137.1199 (loss of phenylthiadiazole moiety; $C_9H_{15}N^{\cdot+}$), *m/z* 211.0897 (loss of the phenylmethanimine moiety; $C_{10}H_{15}N_2OS^+$), and *m/z* 254.1649 (1, 3 rearrangement of ABT-126, followed by loss of SCH_2O; $C_{16}H_{20}N_3^+$). Proposed fragmentation pathways of ABT-126 are provided in Supplemental Figure 1.

M1. The metabolite M1 produced a protonated molecular ion at *m/z* 330.1274, indicating the addition of one oxygen atom to the parent drug (calculated mass *m/z* 330.1271; $C_{17}H_{20}N_3O_2S^+$). The CID of M1 (*m/z* 330) produced the key fragment ions at *m/z* 152.1071 (loss of phenylthiadiazole moiety) and *m/z* 136.1122 (further loss of oxygen from *m/z* 152), suggesting that oxidation occurred at aza-adamantane nitrogen. M1 was assigned as an *N*-oxide metabolite of ABT-126. The structure of M1 was further confirmed by comparing MS/MS fragmentation

pattern and chromatographic retention time with the reference standard. Proposed fragmentation pathways of M1 are provided in Supplemental Figure 1.

M11. The metabolite M11 produced a protonated molecular ion at *m/z* 490.1642, suggesting the addition of a glucuronide to the parent drug (calculated mass *m/z* 490.1643; $C_{23}H_{28}N_3O_7S^+$). The major fragment of M11 was *m/z* 314.1318 (loss of glucuronide). M11 was assigned as a quaternary *N*-glucuronide of ABT-126. The structure of M1 was further confirmed by comparing MS/MS fragmentation pattern and chromatographic retention time with the reference standard.

M12. The metabolite M12 produced a protonated molecular ion of *m/z* 476.1848, indicating the addition of a glucose to the parent drug (calculated mass *m/z* 476.1850; $C_{23}H_{30}N_3O_6S^+$). The major fragment of M12 was *m/z* 314.1317 (loss of glucose). M12 was assigned as quaternary *N*-glucose conjugate of ABT-126. The structure of M12 was further confirmed by comparing MS/MS fragmentation pattern and chromatographic retention time with the reference standard.

Metabolite Profile from Hepatocyte Incubations

Following incubations of [^{3}H]ABT-126 in rat, dog, monkey and human hepatocytes (1 μM, 0-4 hour), ABT-126 showed highest intrinsic clearance in dog (4.8 L/hr/kg). The intrinsic clearance was lower in human, monkey, and rat (~1.0 L/hr/kg). M1 was the primary metabolite in the test species, representing 25.4% (human), 47.4% (monkey), 92.1%, (dog) and 42.8% (rat) of total drug related material after 4 hr incubations, respectively. M11 was observed in human (18.4%) and monkey (9.4%) hepatocytes but not in dog and rat hepatocytes. In addition, a trace amount of M12 was detected only in human hepatocyte incubations by LC-MS.

Metabolism of ABT-126 with cDNA-Expressed Cytochrome 450 and FMO Enzymes

DMD Fast Forward. Published on January 18, 2018 as DOI: 10.1124/dmd.117.077511
This article has not been copyedited and formatted. The final version may differ from this version.

Incubations of [^{3}H]ABT-126 with human cDNA-expressed cytochrome P450 (CYP1A2, 2A6, 2B6, 2C8, 2C9, 2C18, 2C19, 2D6, 2E1, 3A4) or FMO enzymes (FMO1, FMO3, and FMO5) at 37 ^{o}C for 60 minutes indicated that several enzymes were capable of metabolizing ABT-126 to form M1. These enzymes included CYP3A4 (10% conversion to M1), 2D6 (2.1% conversion to M1), 2B6 (3.2% conversion to M1), FMO1(100% conversion to M1), and FMO3 (100% conversion to M1). Kinetic studies (Figure 7) were conducted to determine the K_m and V_{max} values for M1 formation with cDNA-expressed FMO1 and FMO3. M1 formation catalyzed by FMO1 and FMO3 exhibited Michaelis-Menten kinetics with apparent K_m values of 12.5 μM and 89.4 μM, V_{max} values of 2610 pmol/minute/mg protein and 2870 pmol/minute/mg protein, and CL_{int} values of 0.21 μL/minute/mg and 0.032 μL/minute/mg, respectively (Table 4).

Metabolism of ABT-126 with cDNA-Expressed UGT Enzymes.

A panel of recombinant UGT enzymes (UGT1A1, 1A3, 1A4, 1A6, 1A7, 1A9, 1A10, 2B4, 2B7, 2B10, 2B15, and 2B17) was incubated with [^{3}H]ABT-126 (37 ^{o}C for 60 minutes). Parent turnover was observed only with UGT1A4 and UGT2B10 only. Follow-on kinetic studies were conducted to determine the K_m and V_{max} values for M11 formation with these two enzymes. Biphasic kinetics was observed for M11 formation by UGT1A4 (Figure 8). The high-affinity component exhibited apparent K_m, V_{max} and CL_{int} values of 0.232 μM, 0.613 pmol/minute/mg, and 0.0026 μL/minute/mg, respectively, whereas the low-affinity component showed apparent K_m, V_{max}, and CL_{int} values of 115 μM, 123 pmol/minute/mg, and 0.0011 μL/minute/mg, respectively (Table 4). M11 formation by UGT2B10 best fit to one-enzyme Michaelis-Menten kinetics, with an apparent K_m, V_{max} and CL_{int} values of 0.504 μM, 0.17 pmol/minute/mg, and 0.00034 μL/minute/mg, respectively (Table 4).

Metabolism of ABT-126 after thermal treatment of HKM and HLM

Expression of FMO3 and FMO5 is dominant in human liver microsomes, whereas FMO1 is absent. In contrast, human kidney microsomes are rich in FMO1, but not other FMO isoforms (Phillips and Shephard, 2017). Therefore it was of interest to 1) confirm metabolism to M1 *N*-oxide metabolite in these tissue preparations and 2) inhibit M1 formation by mild heat treatment, a process known to inactivate FMO, but not P450 (Grothusen et al, 1996). As anticipated, we observed robust formation of M1 *N*-oxide formation in both HLM and HKM and that the rate of M1 *N*-oxide formation declined substantially (~ 80%, Table 5) upon heat treatment. Benzydamine, a known substrate of FMO1 and FMO3 was used as a positive control and gave the expected response with and without heat treatment (Supplemental table 1). The presence of small but detectable M1 in 0 minute incubations is probably indicative of a small amount of M1 impurity in the starting substrate.

Discussion

Following oral administration of [^{14}C] ABT-126 in healthy subjects, mean total recovery was 94.0% (± 2.09%) over the 216 hours post dose. A mean of 81.5% (± 10.2%) of administered radioactivity was excreted in urine, indicating good oral absorption of ABT-126. ABT-126 was cleared by metabolism and renal excretion (90% and 10%, respectively), with an oral clearance (CL/F) of 42.8 L/hr. Oral bioavailability for ABT-126 in humans was 50%, estimated based on the observed oral bioavailability in rat, dog, and monkey. Thus, the total plasma, renal and metabolic clearance values were estimated to be 21 L/hr, 2 L/hr, and 19 L/hr, respectively. The renal clearance of 2 L/hr indicates that renal elimination of ABT-126 is mainly via glomerular filtration (fraction unbound fu * glomerular filtration rate (GFR)=2.3 L/hr, where fu=0.3 and GFR=125 mL/min). The primary metabolic transformations of ABT-126 include aza-adamantane *N*-oxidation (M1, 50.3% in urine) and aza-adamantane *N*-glucuronidation (M11,

19.9% in urine). M1 and M11 were major circulating components, representing 32.6% and 36.6% of total plasma radioactivity (0-48 hour), which was consistent with the ~3-fold higher plasma concentrations of total radioactivity as compared to those of ABT-126 (measured by LC-MS/MS). The scaled in vitro intrinsic clearance from human hepatocytes (22 L/hr) was similar to the estimated in vivo metabolic clearance (19 L/hr) noted earlier. These data suggest that metabolic clearance of ABT-126 is primarily mediated by hepatic enzymes.

N-oxidation is a commonly observed metabolic pathway catalyzed by FMO, but also by cytochrome P450 enzymes. Example tertiary amines undergoing *N*-oxidation by FMO include tamoxifen, cimetidine, clozapine, itopride and imipramine (Phillips and Shephard, 2017). Compared to CYPs, FMOs exhibit a preference for substrates exhibiting greater nucleophilicity or basicity (Phillips and Shephard, 2017). ABT-126 contains a nucleophilic and basic nitrogen with a pKa value of 9; consistent with our findings of that M1 is primarily formed by cDNA-expressed FMO1 and FMO3 with only a minor contribution from CYP3A4 and 2D6. Our studies demonstrating *N*-oxidation in HLM and HKM, and that these catalytic activities could be suppressed by mild heat inactivation further confirm roles for FMO3 and FMO1 in ABT-126 metabolism. Additionally, the absence of significant CYP3A4 involvement was confirmed by a clinical DDI study with ketoconazole showing that ABT-126 exposures (75 mg) were not affected by ketoconazole (200 mg BID) (AbbVie internal data). Kinetic studies showed V_{max} values for M1 formation by cDNA-expressed FMO1 and FMO3 were comparable, but FMO1 exhibited approximately 7-fold higher affinity and intrinsic clearance as compared with FMO3. FMO1 is the most prevalent FMO in human kidney but absent in adult human liver whereas FMO3 is the predominant FMO isoform in human liver (Cashman and Zhang, 2006). Despite FMO1 exhibiting high abundance in kidney, after estimating expression and controlling for

tissue weight, it has been estimated that the overall abundance of FMO1 is approximately 33-fold less than FMO3 (Overby et al., 1997; Yeung et al., 2000; Zhang and Cashman, 2006). Despite the observation of higher catalytic efficiency of FMO1 toward ABT-126, the significantly lower abundance this enzyme in comparison to FMO3 suggests that M1 is primarily generated by human FMO3 after oral administration. Unfortunately, quantitative contribution of FMO1 and FMO3 to M1 formation and overall ABT-126 clearance is uncertain due to the lack of scaling factors or well-established methods to extrapolate in vitro data to clinical observations. Recent progress using hepatocytes and heat deactivated or chemically inhibited HLM is encouraging (Jones et al, 2017). Further studies are warranted to determine the ISEF values for cDNA-expressed FMO1 and FMO3 to extrapolate activity from these recombinant systems to the activity present in HLM or HKM.

From the perspective of drug-drug interactions, significant contribution of FMO enzymes to the metabolism of ABT-126 is considered attractive. This is because FMO is not readily induced or inhibited by environmental chemicals or drugs (Cashman and Zhang, 2006) and therefore ABT-126 clearance is unlikely to be affected by co-medications. Similarly, significant drug-drug interactions arising with substrates of UGT enzymes are unlikely (William and Hyland, 2004) therefore the role of UGTs in ABT-126 metabolism is likely to further reduce potential DDI liabilities.

The formation of the other major human metabolite aza-adamantane *N*-glucuronide (M11) was found to be mediated by UGT1A4 and UGT2B10. UGT1A4 has been known to catalyze quaternary *N*-glucuronidation of substrates incorporating aliphatic tertiary amine or aromatic *N*-heterocyclic group including tricyclic antidepressants (TCAs), nicotine, nitrosamines (Green et al., 1995; Green and Tephly, 1998; Kubota et al., 2007). Recent studies have indicated that

UGT2B10 may also play an important role in catalyzing quaternary *N*-glucuronidation reactions (Zhou et al., 2010; Fowler et al., 2015; Pattanawongsa et al., 2016), and often displays a lower Km than UGT1A4. In the present study, UGT1A4 exhibited approximately 11-fold higher intrinsic clearance than UGT2B10 for M11 formation. Because hepatic abundance of UGT1A4 and UGT2B10 in human liver is similar (Sato et al., 2014), the higher intrinsic clearance exhibited by UGT1A4 strongly suggests M11 is mainly generated by human UGT1A4 with a lesser role for UGT2B10.

Notable species dependent formation of M11 was observed in hepatocytes. After a 4 hour incubation, M11 was formed in human (18.4%) and monkey (9.4%) but not in dog or rat hepatocytes. Quaternary *N*-glucuronidation is commonly observed in human and non-human primate, but usually absent or minimal in rodents and dog, which is consistent with our observations (Chiu and Huskey, 1998). Indeed, UGT1A4 is a nonfunctional pseudogene in rat and mouse that may explain the low activities in rodents (Mackenzie et al., 2005). An orthologue of UGT2B10 has not yet been characterized in preclinical species suggesting that UGT2B10 plays an important role in the *N*-glucuronidation reactions in human and non-human primates only (Kaivosaari et al., 2011).

It is interesting to note that *N*-oxidation and/or *N*-glucuronidation reactions observed with ABT-126 were similar to those observed for other α7 nAChR agonists that contain a quinuclidine ring (similar to aza-adamantane ring) including PHA-568487 (Shilliday et al., 2010), AZD0328, and N-(3R)-1-azabiocycl[2.2.2]ot-3-ylfuro[2,3-c]pyridine-5-carboxamide (1) (Shaffer et al., 2007) and ABT-107 (Liu et al., 2013)

M1 and M11 are not expected to be pharmacologically active in vivo in human as both metabolites exhibited essentially no in vitro activation of human α7 nAChR (>50-fold less potent

than ABT-126) at concentrations up to 100 μM, and no activation or inhibition of human α4β2, or activation of α3β4. Furthermore, M1 and M11 were evaluated in an extensive receptor binding panel that included G-protein coupled receptors, ion channels, transporters, and are not expected to have clinically relevant off-target pharmacologic activity. In addition, the plasma quantification of M1 at steady state in human (100 mg, QD) and in rats, dogs, and monkeys at NOAEL doses showed adequate coverage of M1 in these preclinical safety species.

In summary, this AME study with [^{14}C]ABT-126 in healthy adult subjects showed that ABT-126 exhibits high absorption (>81.5% of the administered dose), extensive metabolism, and was excreted renally (94% of the administered dose). ABT-126 was predominantly cleared by metabolism, through aza-adamantane *N*-oxidation (M1) and aza-adamantane *N*-glucuronidation (M11). M1 formation is catalyzed by human liver FMO3 and to a lesser extent by human kidney FMO1 while M11 formation is attributed to UGT1A4 with a minor role for UGT2B10.

Authorship Contributions

Participated in research design: Liu, Stresser, Othman

Conducted experiments: Michmerhuizen, Li,

Contributed new reagents: Reed, Schrimpf

Performed data analysis: Liu, Michmerhuizen, Stresser, Li, Othman

Wrote or contributed to the writing of the manuscript: Liu, Stresser, Li, Michmerhuizen, Lee, Sydor

References

Alzheimer's A (2016) 2016 Alzheimer's disease facts and figures. *Alzheimer's & dementia : the journal of the Alzheimer's Association* **12:**459-509.

Cashman JR and Zhang J (2006) Human flavin-containing monooxygenases. *Annual review of pharmacology and toxicology* **46:**65-100.

Chiu SH and Huskey SW (1998) Species differences in N-glucuronidation. *Drug metabolism and disposition* **26:**838-847.

Deardorff WJ, Shobassy A, and Grossberg GT (2015) Safety and clinical effects of EVP-6124 in subjects with Alzheimer's disease currently or previously receiving an acetylcholinesterase inhibitor medication. *Expert review of neurotherapeutics* **15:**7-17.

Florian H, Meier A, Gauthier S, Lipschitz S, Lin Y, Tang Q, Othman AA, Robieson WZ, and Gault LM (2016) Efficacy and Safety of ABT-126 in Subjects with Mild-to-Moderate Alzheimer's Disease on Stable Doses of Acetylcholinesterase Inhibitors: A Randomized, Double-Blind, Placebo-Controlled Study. *Journal of Alzheimer's disease : JAD* **51:**1237-1247.

Fowler S, Kletzl H, Finel M, Manevski N, Schmid P, Tuerck D, Norcross RD, Hoener MC, Spleiss O, and Iglesias VA (2015) A UGT2B10 splicing polymorphism common in african populations may greatly increase drug exposure. *The Journal of pharmacology and experimental therapeutics* **352:**358-367.

Gault LM, Lenz RA, Ritchie CW, Meier A, Othman AA, Tang Q, Berry S, Pritchett Y, and Robieson WZ (2016) ABT-126 monotherapy in mild-to-moderate Alzheimer's dementia: randomized double-blind, placebo and active controlled adaptive trial and open-label extension. *Alzheimer's research & therapy* **8:**44.

Gault LM, Ritchie CW, Robieson WZ, pritchett Y, Othman AA, and Lenz RA (2015) A phase 2 randomized, controlled trial of the α7 agonist ABT−126 in mild-to-moderate Alzheimer's

dementia. *Alzheimer's & Dementia: Translational Research & Clinical Interventions* **1:**81-90.

Gotti C and Clementi F (2004) Neuronal nicotinic receptors: from structure to pathology. *Progress in neurobiology* **74:**363-396.

Green MD, Bishop WP, and Tephly TR (1995) Expressed human UGT1.4 protein catalyzes the formation of quaternary ammonium-linked glucuronides. *Drug metabolism and disposition* **23:**299-302.

Green MD and Tephly TR (1998) Glucuronidation of amine substrates by purified and expressed UDP-glucuronosyltransferase proteins. *Drug metabolism and disposition* **26:**860-867.

Grothusen A, Hardt J, Bräutigam L, Lang D and Böcker R (1996) A convenient method to discriminate between cytochrome P450 enzymes and flavin-containing monooxygenases in human liver microsomes. *Arch. Toxicol.* **71**: 64–71

Haig G, Wang D, Othman AA, and Zhao J (2016a) The alpha7 Nicotinic Agonist ABT-126 in the Treatment of Cognitive Impairment Associated with Schizophrenia in Nonsmokers: Results from a Randomized Controlled Phase 2b Study. *Neuropsychopharmacology : official publication of the American College of Neuropsychopharmacology* **41:**2893-2902.

Haig GM, Bain EE, Robieson WZ, Baker JD, and Othman AA (2016b) A Randomized Trial to Assess the Efficacy and Safety of ABT-126, a Selective alpha7 Nicotinic Acetylcholine Receptor Agonist, in the Treatment of Cognitive Impairment in Schizophrenia. *The American journal of psychiatry* **173:**827-835.

Hamilton RA, Garnett WR, and Kline BJ (1981) Determination of mean valproic acid serum level by assay of a single pooled sample. *Clinical pharmacology and therapeutics* **29:**408-413.

Kaivosaari S, Finel M, and Koskinen M (2011) N-glucuronidation of drugs and other xenobiotics by human and animal UDP-glucuronosyltransferases. *Xenobiotica* **41:**652-669.

Jones BC, Srivastava A, Colclough N, Wilson J, Reddy VP, Amberntsson S, Li D (2017) An investigation into the prediction of in vivo clearance for a range of Flavin-containing monooxygenase substrates. *Drug metabolism and disposition* DOI: 10.1124/dmd.117.077396

Kubota T, Lewis BC, Elliot DJ, Mackenzie PI, and Miners JO (2007) Critical roles of residues 36 and 40 in the phenol and tertiary amine aglycone substrate selectivities of UDP-glucuronosyltransferases 1A3 and 1A4. *Molecular pharmacology* **72:**1054-1062.

Lendvai B, Kassai F, Szajli A, and Nemethy Z (2013) alpha7 nicotinic acetylcholine receptors and their role in cognition. *Brain research bulletin* **93:**86-96.

Liu H, Deng X, Liu J, Liu N, Stuart P, Xu H, Guan Z, Marsh KC, and De Morais SM (2013) Species-dependent metabolism of a novel selective alpha7 neuronal acetylcholine receptor agonist ABT-107. *Xenobiotica* **43:**803-816.

Mackenzie PI, Bock KW, Burchell B, Guillemette C, Ikushiro S, Iyanagi T, Miners JO, Owens IS, and Nebert DW (2005) Nomenclature update for the mammalian UDP glycosyltransferase (UGT) gene superfamily. *Pharmacogenetics and genomics* **15:**677-685.

Overby LH, Carver GC, and Philpot RM (1997) Quantitation and kinetic properties of hepatic microsomal and recombinant flavin-containing monooxygenases 3 and 5 from humans. *Chemico-biological interactions* **106:**29-45.

Pattanawongsa A, Nair PC, Rowland A, and Miners JO (2016) Human UDP-Glucuronosyltransferase (UGT) 2B10: Validation of Cotinine as a Selective Probe Substrate, Inhibition by UGT Enzyme-Selective Inhibitors and Antidepressant and Antipsychotic Drugs, and Structural Determinants of Enzyme Inhibition. *Drug metabolism and disposition* **44:**378-388.

Phillips IR and Shephard EA (2017) Drug metabolism by flavin-containing monooxygenases of human and mouse. *Expert opinion on drug metabolism & toxicology* **13:**167-181.

Roncarati R, Scali C, Comery TA, Grauer SM, Aschmi S, Bothmann H, Jow B, Kowal D, Gianfriddo M, Kelley C, Zanelli U, Ghiron C, Haydar S, Dunlop J, and Terstappen GC (2009) Procognitive and neuroprotective activity of a novel alpha7 nicotinic acetylcholine receptor agonist for treatment of neurodegenerative and cognitive disorders. *The Journal of pharmacology and experimental therapeutics* **329:**459-468.

Sato Y, Nagata M, Tetsuka K, Tamura K, Miyashita A, Kawamura A, and Usui T (2014) Optimized methods for targeted peptide-based quantification of human uridine 5'-diphosphate-glucuronosyltransferases in biological specimens using liquid chromatography-tandem mass spectrometry. *Drug metabolism and disposition* **42:**885-889.

Shaffer CL, Gunduz M, Scialis RJ, and Fang AF (2007) Metabolism and disposition of a selective alpha(7) nicotinic acetylcholine receptor agonist in humans. *Drug metabolism and disposition* **35:**1188-1195.

Shilliday FB, Walker DP, Gu C, Fang X, Thornburgh B, Fate GD, and Daniels JS (2010) Multiple species metabolism of PHA-568487, a selective alpha 7 nicotinic acetylcholine receptor agonist. *Drug metabolism letters* **4:**162-172.

Taniguchi-Takizawa T, Shimizu M, Kume T, and Yamazaki H (2015) Benzydamine N-oxygenation as an index for flavin-containing monooxygenase activity and benzydamine N-demethylation by cytochrome P450 enzymes in liver microsomes from rats, dogs, monkeys, and humans. Drug Metab Pharmacokinet 30:64–69.

Williams JA, Hyland R, Jones BC, Smith DA, Hurst S, Goosen TC, Peterkin V, Koup JR, Ball SE. (2004) Drug-drug interactions for UDP-glucuronosyltransferase substrates: a pharmacokinetic explanation for typically observed low exposure (AUCi/AUC) ratios. *Drug metabolism and disposition* **32:**1201-1208.

Yeung CK, Lang DH, Thummel KE, and Rettie AE (2000) Immunoquantitation of FMO1 in human liver, kidney, and intestine. *Drug metabolism and disposition* **28:**1107-1111.

Zhang J and Cashman JR (2006) Quantitative analysis of FMO gene mRNA levels in human tissues. *Drug metabolism and disposition* **34:**19-26.

Zhou D, Guo J, Linnenbach AJ, Booth-Genthe CL, and Grimm SW (2010) Role of human UGT2B10 in N-glucuronidation of tricyclic antidepressants, amitriptyline, imipramine, clomipramine, and trimipramine. *Drug metabolism and disposition* **38:**863-870.

Disclosure Statement: All authors are employees of AbbVie and may hold AbbVie stock or stock options. AbbVie provided financial support for the studies and participated in the design, study conduct, analysis and interpretation of data as well as the writing, review and approval of the publication.

Figures

Figure 1. Mean plasma concentration-time profiles of total Radioactivity, ABT-126, M1 and M11 in healthy male subjects after a single oral dose of 100 mg of [^{14}C]ABT-126 containing 100 μCi radioactivity.

Figure 2. Mean (± SD) cumulative percentage of radioactive dose recovered in urine and feces at specified intervals after a single oral dose of 100 mg (100 μCi) of [^{14}C]ABT-126 to healthy male subjects.

Figure 3. Representative HPLC radiochromatogram of ABT-126 and its metabolites in human plasma at 6 hours after a single oral dose of [^{14}C]ABT-126 to healthy male subjects.

Figure 4. Representative HPLC radiochromatogram of ABT-126 and its metabolites in human urine after a single oral dose of [^{14}C]126 (24-48 hour post dose).

Figure 5. Representative HPLC radiochromatogram of ABT-126 and its metabolites in human feces after a single oral dose of [^{14}C]ABT-126 (8-24 hour post dose).

Figure 6. Proposed metabolic pathways of ABT-126 in humans.

Figure 7. Kinetic analysis of M1 formation by recombinant FMO1 (A) and FMO3 (B). The rates represent the mean (±SD) of triplicate incubations. An Eadie-Hofstee plot is also presented as an inset for each enzyme.

Figure 8. Kinetic analysis of M11 formation of recombinant UGT1A4 (A) and UGT2B10 (B). The rates represent the mean (±SD) of triplicate incubations. An Eadie-Hofstee plot is also presented as an inset for each enzyme.

Tables

Table 1. Mean (%CV) pharmacokinetic parameters of total radioactivity, ABT-126 and its metabolite in plasma after a single oral dose of [^{14}C]ABT-126

Pharmacokinetic parameters (units)[a]	T_{max} (hour)	C_{max} (ng/mL or ng-eq/g)	$AUC_{(0-t)}$ (hour•ng/mL or hour•ng-eq/g)	$AUC_{0-\infty}$ (hour•ng/mL or hour•ng-eq/g)	$t_{1/2}$[c] (hour)	% Total Radioactivity ($AUC_{0-\infty}$)	% of ABT-126 ($AUC_{0-\infty}$)
ABT-126 [a] (LC-MS/MS)	4.0 (1.6)	89.7 (15.2)	2400 (525)	2440 (532)	33.9 (5.1)	26.2	-
ABT-126[b] (Radioprofiling)	4	101	2190	2620	-	28.5	-
M1[b] (Radioprofiling)	3	159	2260	3000	-	32.6	115
M11[b] (Radioprofiling)	16	72.9	2320	3360	-	36.6	128
Total Radioactivity (LSC) (SD)[a]	4 (1.4)	318 (19)	7400 (1406)	9190 (1746)	-	-	-

a. N=4.

b. Pharmacokinetic parameters for ABT-126 and its metabolites were calculated from pooled samples (pooled per each time point across subjects to that one concentration per time point was obtained for parent and each metabolite)

c. Terminal phase elimination half-life $t_{1/2}$ was not determined for total radioactivity, ABT-126 (radioprofiling), M1 and M11 because radioactivity levels were below LOQ (40.1 ng equivalents/g) in the samples from 72 to 192 hours.

Table 2. Percentages of ABT-126 and metabolites in human urine and feces following a single oral dose of 100 mg (100 μCi) of [^{14}C]ABT-126 (n=4)

Compounds	Urine (0-192 hour)	Feces (0-192 hour)	Total
ABT-126	6.6	12.2	18.8
M1	50.3	MS	50.3
M3	0.9	MS	0.9
M7	MS	N.D.	N.A.
M8	MS	N.D.	N.A.
M10	0.9	N.D.	0.9
M11	19.9	0.2	20.1
M12	1.5	MS	1.5
M16	0.2	N.D.	0.2
UNK1	0.9	N.D.	0.9

MS: Detected in mass spec only; N.D.: Not detected; N.A.: Not applicable

DMD Fast Forward. Published on January 18, 2018 as DOI: 10.1124/dmd.117.077511
This article has not been copyedited and formatted. The final version may differ from this version.

Table 3. Molecular ions and characteristic fragment ions of ABT-126 and metabolites in human plasma, feces and/or urine

Compound	$[M+H]^+$ (Theoretical)	$[M+H]^+$ (Measured)	Δ ppm	Molecular Formula	Key Fragment Ions (*m/z*)
ABT-126	314.1322	314.1325	0.9	$C_{17}H_{20}N_3OS^+$	254, 211, 137, 136, 108
M1	330.1271	330.1274	0.9	$C_{17}H_{20}N_3O_2S^+$	313, 270, 227, 152, 136
M3	346.1220	346.1220	-0.1	$C_{17}H_{20}N_3O_3S^+$	329, 152, 136
M7	426.0788	426.0786	-0.5	$C_{17}H_{20}N_3O_6S_2^+$	346
M8	506.1592	506.1591	-0.2	$C_{23}H_{28}N_3O_8S^+$	330
M10	451.1468	451.1467	-0.2	$C_{20}H_{27}N_4O_4S_2^+$	433, 364, 330, 314, 136
M11	490.1643	490.1642	-0.2	$C_{23}H_{28}N_3O_7S^+$	314
M12	476.1850	476.1848	-0.4	$C_{23}H_{30}N_3O_6S^+$	314
M16	506.1592	506.1592	0	$C_{23}H_{28}N_3O_8S^+$	330, 314

DMD Fast Forward. Published on January 18, 2018 as DOI: 10.1124/dmd.117.077511
This article has not been copyedited and formatted. The final version may differ from this version.

Table 4. Apparent kinetic parameters for *N*-oxidation of ABT-126 by recombinant FMO1 and FMO3 and *N*-glucuronidation of ABT-126 by recombinant UGT1A4 and UGT2B10[a]

	K_m (μM)	V_{max} (pmol/minute/mg)	CL_{int} (μL/minute/mg)	K_{m2} (μM)	V_{max2} (pmol/minute/mg)	CL_{int2} (μL/minute/mg)
FMO1	12.5 (1.8)	2610 (94)	0.21	N.A.	N.A.	N.A.
FMO3	89.4 (15)	2870 (239)	0.032	N.A.	N.A.	N.A.
UGT1A4	0.232 (0.044)	0.613 (0.068)	0.0026	115 (13)	123 (12)	0.0011
UGT2B10	0.504 (0.041)	0.17 (0.003)	0.00034	N.A.	N.A.	N.A.

[a]- Parameter estimates were obtained from data fitted on the mean of triplicate incubations; the standard error of the estimate is shown in parenthesis for K_m and V_{max} parameters

N.A., not applicable

DMD Fast Forward. Published on January 18, 2018 as DOI: 10.1124/dmd.117.077511
This article has not been copyedited and formatted. The final version may differ from this version.

Table 5. Inactivation of M1 formation by thermal treatment of human liver and kidney microsomes.

		M1 Metabolite formation (μM)			
	Substrate	0 minute	15 minute	30 minute	60 minute
HLM	ABT-126	0.071 (0.016) [a]	1.5 (0.068)	3.0 (0.023)	7.6 (1.1)
HLM + heat[b]	ABT-126	0.056 (0.003)	0.33 (0.008)	0.63 (0.012)	1.5 (0.071)
HKM	ABT-126	0.11 (0.012)	1.6 (0.15)	2.8 (0.064)	5.6 (0.61)
HKM + heat	ABT-126	0.045 (0.013)	0.16 (0.028)	0.22 (0.011)	1.3 (0.49)

[a] Mean (SD) of three replicates

[b] Thermal treatment consisted of heating microsomal suspension for 90 seconds at 50 °C prior to inclusion in the assay

DMD Fast Forward. Published on January 18, 2018 as DOI: 10.1124/dmd.117.077511
This article has not been copyedited and formatted. The final version may differ from this version.

Figure 1

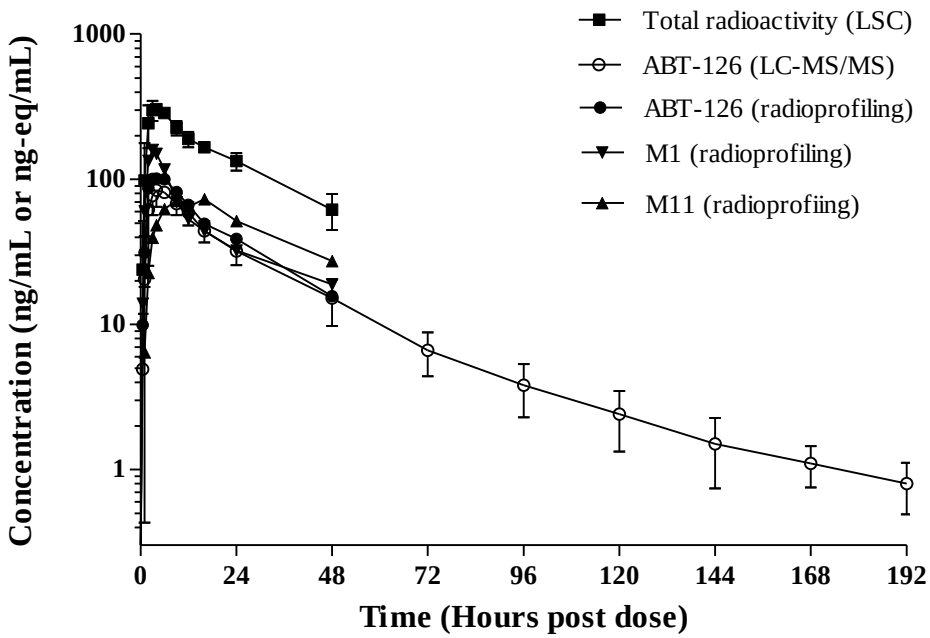

DMD Fast Forward. Published on January 18, 2018 as DOI: 10.1124/dmd.117.077511
This article has not been copyedited and formatted. The final version may differ from this version.

Figure 2

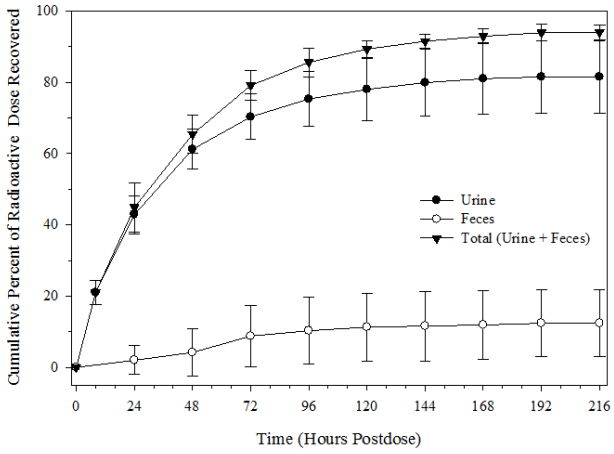

DMD Fast Forward. Published on January 18, 2018 as DOI: 10.1124/dmd.117.077511
This article has not been copyedited and formatted. The final version may differ from this version.

Figure 3

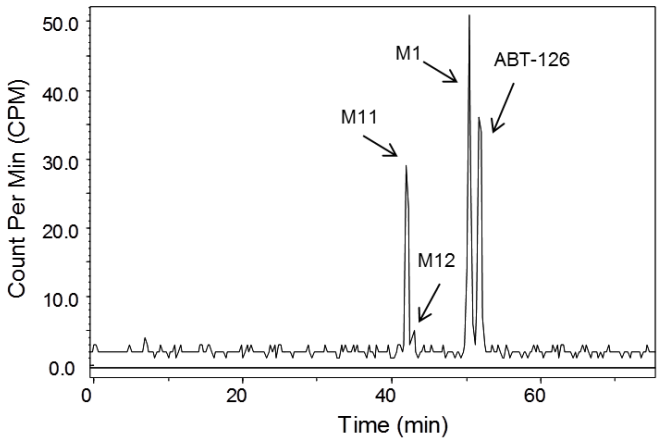

DMD Fast Forward. Published on January 18, 2018 as DOI: 10.1124/dmd.117.077511
This article has not been copyedited and formatted. The final version may differ from this version.

Figure 4

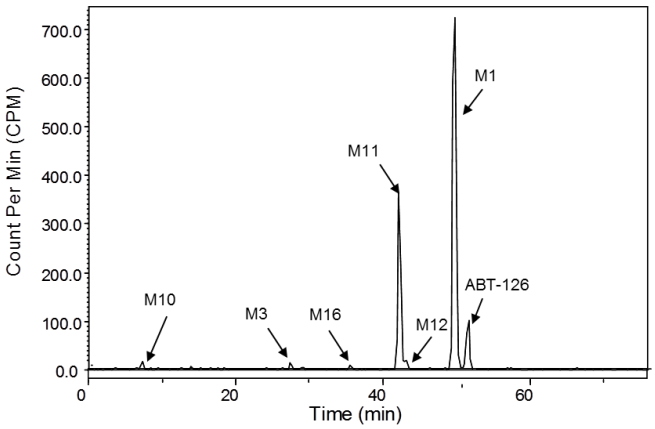

DMD Fast Forward. Published on January 18, 2018 as DOI: 10.1124/dmd.117.077511
This article has not been copyedited and formatted. The final version may differ from this version.

Figure 5

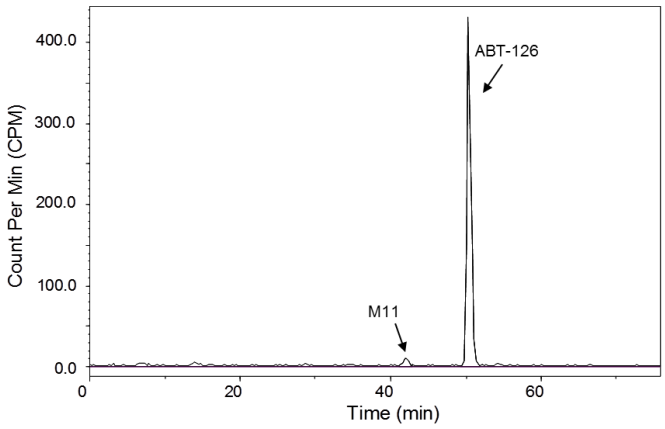

DMD Fast Forward. Published on January 18, 2018 as DOI: 10.1124/dmd.117.077511
This article has not been copyedited and formatted. The final version may differ from this version.

Figure 6

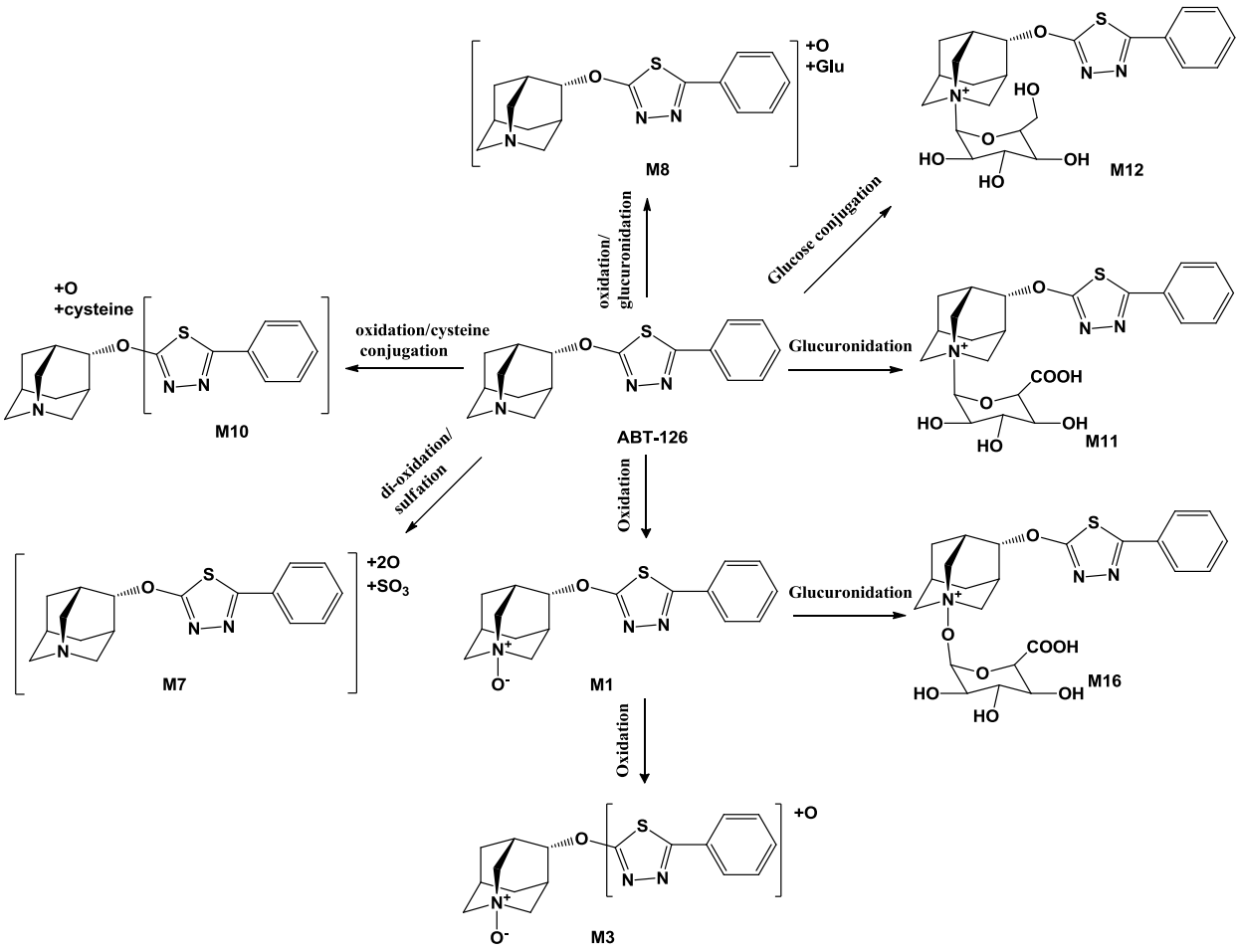

Metabolites including M3, M7, M8, M10, M12, M16 are minor metabolites (each <2% of dose).

DMD Fast Forward. Published on January 18, 2018 as DOI: 10.1124/dmd.117.077511
This article has not been copyedited and formatted. The final version may differ from this version.

Figure 7

A

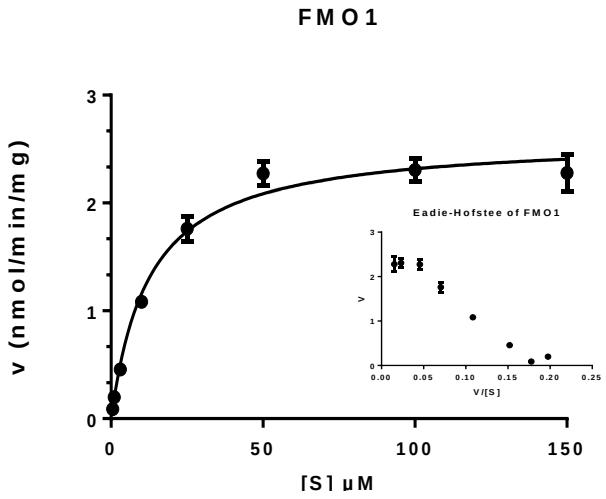

B

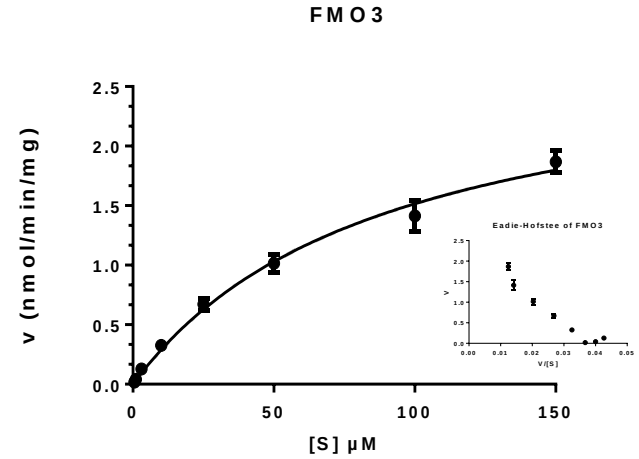

DMD Fast Forward. Published on January 18, 2018 as DOI: 10.1124/dmd.117.077511
This article has not been copyedited and formatted. The final version may differ from this version.

Figure 8

A

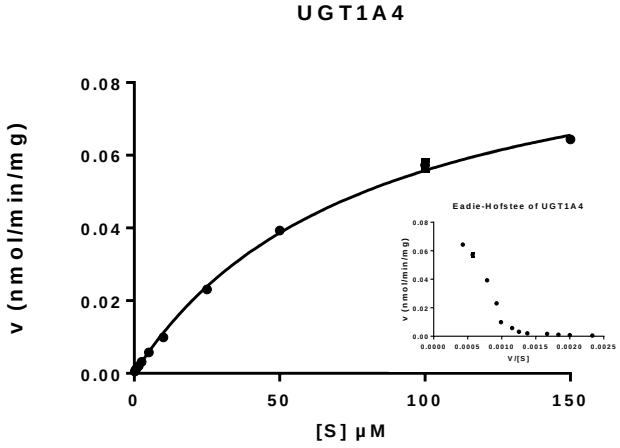

B